Oscillator strength of the peptide bond π^* resonances at all relevant x-ray absorption edges

K. Kummer,[1] V. N. Sivkov,[2] D. V. Vyalikh,[1] V. V. Maslyuk,[3] A. Blüher,[4] S. V. Nekipelov,[2] T. Bredow,[5] I. Mertig,[3] M. Mertig,[4] and S. L. Molodtsov[1]

[1]*Institut für Festkörperphysik, Technische Universität Dresden, D-01062 Dresden, Germany*

[2]*Komi Science Center, Russian Academy of Science, Ural Division, Syktyvkar 167982, Russia*

[3]*Martin-Luther-Universität Halle-Wittenberg, Fachbereich Physik, D-06099 Halle, Germany*

[4]*Max-Bergmann-Zentrum für Biomaterialien und Institut für Werkstoffwissenschaft, Technische Universität Dresden, D-01062 Dresden, Germany*

[5]*Institut für Physikalische und Theoretische Chemie, Universität Bonn, D-53115 Bonn, Germany*

(Received 18 August 2009; revised manuscript received 15 September 2009; published 15 October 2009)

Absolute x-ray absorption cross sections of a regular bacterial surface-layer protein deposited on a naturally oxidized silicon substrate were determined experimentally. Upon separation of the partial cross sections of the three relevant $1s$ absorption edges, the oscillator strengths of the $1s \rightarrow \pi^*$ excitations within the peptide-backbone unit were extracted. Comparison with results of first-principles calculations revealed their close correlation to the topology of $\pi^*_{peptide}$ orbitals of the peptide backbone.

DOI: 10.1103/PhysRevB.80.155433 PACS number(s): 33.20.Rm, 33.80.Eh, 33.70.−w

I. INTRODUCTION

X-ray absorption of molecules, in particular, the near-edge x-ray absorption fine structure (NEXAFS), is closely related to the intramolecular structure.[1] Probing it allows to get insight into fundamental properties such as chemical bonding,[2–4] spatial conformation,[5] or orientation of molecules.[6–8] Accordingly, NEXAFS spectroscopy has become a routine tool in atomic, molecular, and solid-state physics as well as in material science.

Almost exclusively, analysis of x-ray absorption spectra is focused on the energy position of certain spectral features or their relative intensity when compared with other reference spectra. Except for a few experiments which have been conducted in gas cells, severe experimental obstacles mostly hinder a quantitative characterization of the x-ray absorption properties in terms of absorption cross sections. This holds, in particular, for the entire class of ultrathin molecular systems adsorbed to solid surfaces including graphene or biomolecular top layers. In all these cases, the data have to be collected in an electron or fluorescence yield mode. However, deriving x-ray absorption cross sections of a thin molecular top layer from the detected yield signal is far from being straightforward—even on a qualitative scale. But naturally, such data is highly desirable for several reasons. It would allow for quantitative conclusions on internal molecular structures. Based upon quantitative rather than only qualitative agreement between experimental and predicted quantities, it would be even possible to better evaluate different theoretical models.

In the current work we address this issue and present an experimental approach to the determination of x-ray absorption cross sections and oscillator strengths for molecular top layers adsorbed to a solid-state surface. Its feasibility is demonstrated at the example of a bacterial surface-protein layer (S layer) adsorbed to a silicon oxide substrate. Doing so, we were able to describe the x-ray absorption of proteins quantitatively. In particular, we obtain the x-ray absorption oscillator strength of $1s \rightarrow \pi^*_{peptide}$ transitions within the peptide backbone for all relevant absorption edges. Upon comparison with results of also performed first-principles calculations, their close correlation to the topology of the unoccupied electronic structure of the peptide backbone is demonstrated.

II. EXPERIMENT

A. Sample characterization

S layers are regular two-dimensional protein crystals which form the outermost cell envelope component of many prokaryotes in almost all phylogenetic branches of bacteria and archaea.[9,10] In particular, the precise spatial modulation of the physicochemical surface properties of the periodic protein crystal makes them an ideal biological matrix for supramolecular engineering.[11,12]

The samples were prepared by depositing regular S-layer sheets, isolated from the cell walls of *Bacillus sphaericus* NCTC 9602 as described previously,[12] *ex situ* onto naturally oxidized Si substrates (SiO_x/Si). The S-layer sheets exhibit a $p4$ symmetry, a lattice constant of 12.5 nm, and a complex pattern of pores and gaps that are 2 nm wide.[12] They are assembled from a single monomer unit. The typical lateral sheet size is 2–5 μm. The thickness of such a protein monolayer amounts to approximately 5 nm. Surface coverage of up to 90% is routinely achieved as it has been verified by scanning electron microscopy (results not shown).

According to its presently known primary structure,[13] a single protein monomer is composed of 19 out of the 20 standard amino acids. In total, it contains 1228 amino acids and has a molecular weight of ~130 kDa. The protein contains 5864 carbon, 1891 oxygen, 4 sulfur, and 1517 nitrogen atoms. This corresponds to 3.87 carbon, 1.24 oxygen, and the neglectable amount of 0.0026 sulfur atoms per one atom of nitrogen. 83% of the nitrogen, 21% of the carbon, and 32% of the oxygen atoms are part of the peptide groups in the protein backbone, the rest is incorporated in the protein side chains. Using linearly polarized light and different angles of

light incidence we found no polarization-dependent behavior in the fine structure of the C, N, and O 1*s* x-ray absorption edges.[14] Thus we conclude that bonds, in particular, in the peptide units, show no preferred orientation within the protein layer.

Particular focus was drawn to thorough cleaning of the naturally oxidized Si wafers serving as substrates. Shortly before sample preparation the substrates were subject to Ar sputtering and immediately prior to S-layer deposition they were additionally plasma treated (RF power 20 W, 5 min, pressure of ambient gases of 1×10^{-2} mbar). In this way contributions of surface contaminations to the measured fine structures were tried to minimize.

B. X-ray absorption spectroscopy

All presented data were obtained at the Berliner Elektronenspeicherring für Synchrotronstrahlung (BESSY) using radiation from the Russian-German beamline (RGBL).[15,16] This dipole beamline was proven to be highly suited for spectroscopic investigations on "fragile" organic and biological molecules[14,17,18] which generally show enhanced sensitivity to x-ray damage effects.[18–20]

All spectra were acquired in total electron yield (TEY) mode by recording the sample drain current. Energy calibration was done for each spectrum using the energy separation between the first- and second-order light-excited Au $4f_{7/2}$ photoemission line taken from a clean gold plate which was additionally mounted to the sample holder. The spectral dependence of the photon flux was determined using a clean Si photocathode. Its cleanliness had been checked before by x-ray photoelectron spectroscopy. We determined the photon flux (in arbitrary units) from the TEY curve of the Si plate by division by the well-known atomic x-ray absorption cross section of Si.[21] At the time of our experiment the flux curve of the RGBL exhibited dips in the photon energy range of O 1*s* excitations (530–570 eV) due to oxygen contamination of the optical elements. This involves the risk to introduce artificial features to the spectra upon normalization because then the background signal is much larger than the sample signal. Hence, we decided to repeat measurements in the O 1*s* range at the beamline D1011 of the MAX II storage ring at MAX-lab (Lund University, Sweden). After normalization to the respective photon flux curves, the spectra showed exactly the same shape regardless at which of both beamlines they were obtained.

C. Light monochromatization and photon flux

Despite its highly monochromatic character, x-ray radiation delivered by the RGBL, and by any beamline, in general, still contains nonmonochromatic portions, i.e., wavelengths deviating from that given by the monochromator settings. This mainly involves parasitic light passing the plane-grating monochromator in higher diffraction orders but also long-wavelength stray radiation. The calculated RGBL transmission ratio between high-order and first-order light is shown in Fig. 1 for different fixed-focus constants $c_{ff} = \cos\beta/\cos\alpha$, where α and β are the incidence and diffraction angle relative to the grating normal, respectively. Obviously, high-order light suppression works best for low c_{ff} values. The fix-focus constant, however, does not only define the transmission ratio but also photon flux and resolving power of the RGBL. While the photon flux increases the resolving power declines for lower c_{ff} values.[15] The best compromise is usually found at c_{ff}=2.25, which was also used during our measurements.

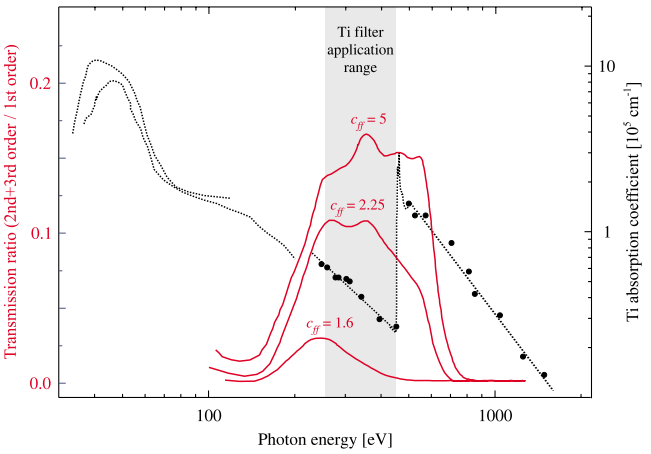

FIG. 1. (Color online) Calculated transmission ratio of the RGBL together with the absorption coefficient of titanium. In the Ti filter application range between 230 and 450 eV long-wavelength and high-order light are strongly suppressed by the filter.

For this c_{ff} value, however, the percentage of high-order light easily reaches more than 10% in the relevant photon energy range. In consequence, it generates a considerable part of the detected TEY to an unknown measure. Since we seek for the x-ray absorption cross section as a function of defined photon energy this undesired, nonmonochromatic contribution must be removed. Recently, we demonstrated that this experimental challenge can be overcome by inserting a titanium filter between beamline and analytical chamber.[22,23] Titanium shows high absorption in the photon energy ranges of 10–100 eV and 450–900 eV (Refs. 24–27) and at the same time good transmission between 250 and 450 eV (see Fig. 1). Therefore, using a Ti filter prepared in the form of a free-standing film we removed both high-order light and long-wavelength stray radiation in the considered photon energy window between 250 and 450 eV.

This is illustrated in Fig. 2, where we show the TEY signal of the Si photocathode as a function of photon energy, once when the Ti filter was mounted and once when it was absent. In the latter case, the pronounced breakdown in TEY in the O 1*s* region is repeated in second order in the photon energy range around 268 eV. This unambiguously proves the presence of considerable shares of high-order light. In contrast, a second-order copy of the O 1*s* structure is not observed when the Ti filter is mounted proving effective suppression of nonmonochromatic light contingents. All further presented spectra were recorded with applied Ti filter.

III. X-RAY ABSORPTION CROSS SECTION OF THE PROTEIN LAYER

A. Spectral dependence

Figure 3 shows the TEY signal obtained from the surface-adsorbed protein monolayer after normalization to the inci-

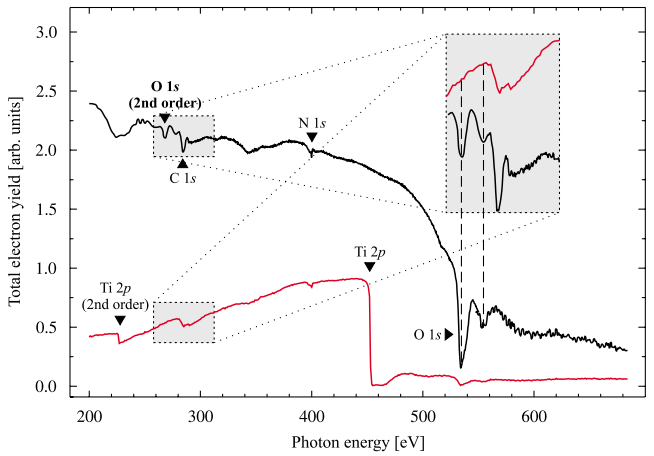

FIG. 2. (Color online) TEY signal taken from a Si photocathode without and with the Ti filter applied [black (upper) and red (lower) line, respectively]. The presence of a second-order light copy of the pronounced O 1*s* structure illustrates considerable impact of nonmonochromatic radiation contingents in the considered photon energy range. They are, however, removed when the Ti filter is introduced into the optical path of the RBGL.

dent photon flux. The curve features distinct jumps when passing the C, N, and O 1*s* edges. More precisely, at each absorption edge it exhibits a near-edge fine structure followed by a monotonically descending tail. While the NEXAFS reflects transitions into unoccupied molecular electronic states, the structureless tail is due to transitions into continuum states far beyond the vacuum level.[1] Between 450 and 475 eV photon energy no experimental data is shown because strong Ti 2*p* absorption extremely attenuated photon flux there. This led to both a very weak and thus noisy sample and reference spectrum, causing the normalized spectrum in this energy range to suffer from very bad statistics.

Measured, flux-normalized electron-yield curves are often considered as replica of the corresponding x-ray absorption

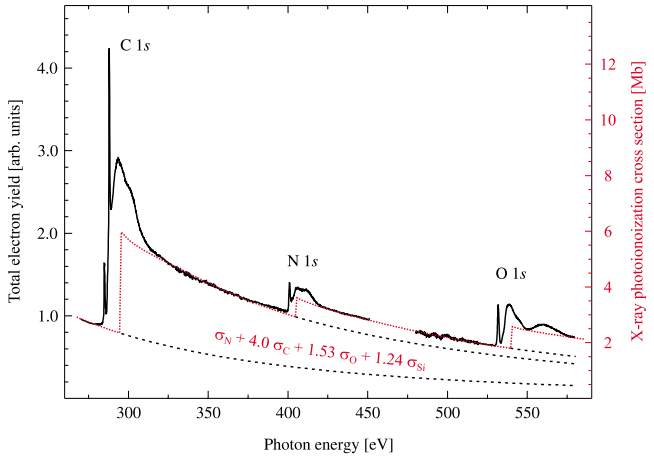

FIG. 3. (Color online) Spectral dependence of the TEY signal after normalization to the incident photon flux. The steps and continuum tails in the spectrum are well described by calculated atomic cross sections σ_x weighted with an assumed chemical composition of $NC_{4.0}O_{1.53}Si_{1.24}$ (dotted, red line). 1 *s* partial signals can be extracted by subtraction of the sum of the calculated atomic cross sections of all lower-lying edges (dashed lines).

cross-section curves. Although there is some evidence for a close similarity between electron-yield and x-ray absorption,[28] this cannot be taken as granted from the beginning, in particular, since comprehensive studies on this point are lacking. For instance, inelastic scattering of primary electrons might release a considerable fraction of secondary electrons. Since the probability for such processes grows monotonically with the electron kinetic energies involved, this could lead to an energy-dependent multiplication of the electron yield.[28] In consequence, in some cases the electron yield might considerably deviate from the x-ray absorption.

However, beside the strong evidence in the already mentioned previous studies,[28] our data itself indicates direct scaling between the curve in Fig. 3 and the total x-ray absorption cross section of the sample. In fact, using atomic calculations of photoionization cross sections,[21] we were able to reproduce the steps and continuum tails of the measured spectrum. Note that for light elements with $Z<10$ the fluorescent decay channel is largely suppressed and photoionization and x-ray absorption cross section can be identified with each other.[29] The best agreement was found when weighting the calculated cross sections σ_x with a relative atomic composition of N/C/O/Si=1/4.0/1.53/1.24. The corresponding curve is included in Fig. 3 as a dotted, red line. Note the close similarity in the regions of continuum transition where atomic calculations hold full validity.[1]

This finding comes along with some severe implications. First and foremost, it contradicts a notable energy dependence of multiplication effects in the considered soft x-ray range, which might have broken the strict proportionality between x-ray absorption and electron yield. Otherwise the slope of the continuum tails would have become flatter with growing photon energies because of the interference of a monotonically increasing background.[28] In consequence, the curve could not be reproduced by atomic cross sections across the entire probed energy range.

Second, the found atomic composition N/C/O/Si =1/4.0/1.53/1.24 well fits the relative atomic composition of the S-layer protein (N/C/O=1/3.87/1.24) given that the additional signal C/O/Si=0.13/0.29/1.24 is easily assigned to contributions by the SiO_x/Si substrate. Though within our experimental uncertainty, we believe that the small rest contribution at the C 1*s* edge is probably caused by substrate contaminations. Repeating measurements on blank substrates we found a tiny signal at the C 1*s* edge with an intensity less than 4% compared to that of substrate *plus* protein layer.

We should mention that so-called saturation effects, which are observed when the effective x-ray penetration depth becomes comparable to the electron escape depth, can also preclude quantitative analysis of electron-yield spectra.[30] In the present case, where 1*s* absorption by light elements is considered, these effects are negligible. They can, however, become severe when 2*p* edges of transition metals are involved.

In summary, we conclude that in the considered soft x-ray range the flux-normalized TEY curve in Fig. 3 indeed represents the spectral dependence of the x-ray absorption of the protein layer on the SiO_x surface. We would like to emphasize that this result is only observed with applied Ti filter, i.e., after full monochromatization of the incident light. The

good agreement between the found atomic composition and the primary structure of the protein also indicates high sample quality.

B. Normalization to the absolute scale

X-ray absorption is quantified either in terms of the absorption cross sections σ or oscillator strengths f. While the former are defined for each photon energy, the latter are a measure for the overall absorption by, e.g., a particular resonance. Both are connected by the well-known relation,[31]

$$\sigma(E) = \left(\frac{8\pi^2\alpha\hbar^2}{m}\right)\frac{df}{dE} = (109.8\ \text{Mb eV})\frac{df}{dE} \qquad (1)$$

with α the fine-structure constant and m the free-electron mass.

Owed to several unknown quantities, it is considered to be nearly impossible to give experimental cross-section curves on an absolute scale in values of megabarn and/or for a single molecule, from electron-yield measurements of surface-adsorbed molecules. To this end, a valid model of all involved processes, including penetration depth of the incident x rays, quantum efficiency for electron excitation and mean escape depth of the excited electrons, would be required. Furthermore, reliable information on the molecule density at the irradiated sample spot and the divergence and internal intensity distribution of the incident beam which are difficult to obtain, should be available.

Here we follow a pragmatic approach where we consider the protein molecule as being assembled from many entities of the average polyatomic group $NC_{3.87}O_{1.24}$. Each chemical complex in the protein is included in this average polyatomic group to a well-known extent, according to its relative occurrence in the protein structure. Having the absolute x-ray absorption cross section for a single $NC_{3.87}O_{1.24}$ entity at hand, one would also be able to calculate cross sections and oscillator strengths for certain chemical groups or the entire protein by reassembling the protein from the average polyatomic group according to its primary structure.

Thus, as the first step, we normalized the measured x-ray absorption curve, which reflects the spectral dependence of x-ray absorption of both average protein entity ($NC_{3.87}O_{1.24}$) and a corresponding average group accounting for the substrate contributions ($C_{0.13}O_{0.29}Si_{1.24}$) together. To this end, we exploited the fact that the excitation probability of continuum transitions far beyond an absorption edge does not depend on the concrete structure of unoccupied molecular states, i.e., molecule properties but is in first approximation a function of photon energy only.[1] By approximation of the continuum tail regions using existing atomic calculations (cf. Fig. 3), one simultaneously normalizes the full signal to absolute x-ray absorption cross sections.[32] We can thus simply assume the right-hand scale in Fig. 3 for the entire measured spectrum.[33] 1*s* partial cross section of each particular absorption edge can be obtained by subtraction of the sum of the calculated atomic cross sections[21] of all lower-lying edges, indicated in Fig. 3 as dashed lines.

With the x-ray absorption cross section for the average protein entity at hand, we now turn to a discussion of the fine structure of all three 1*s* edges. From that, we will try to extract the oscillator strength of the $1s \rightarrow \pi^*_{peptide}$ excitations within the peptide group, which are a characteristic of all protein spectra.

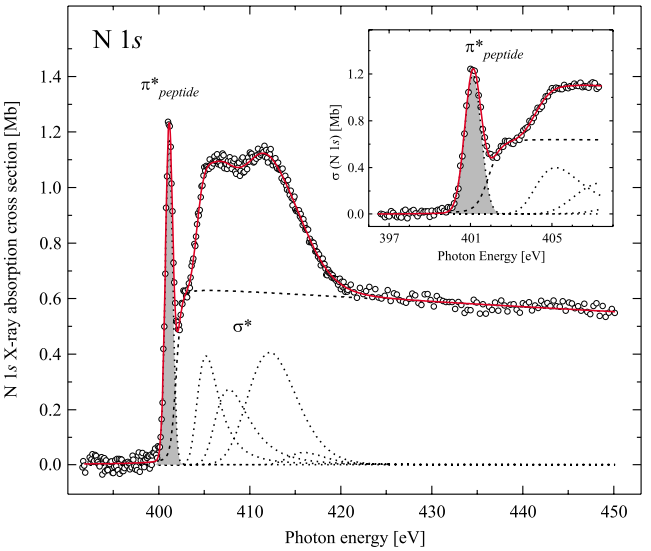

FIG. 4. (Color online) N 1*s* partial x-ray absorption cross section normalized to the contribution of a single nitrogen atom. The sharp resonance at 401.3 eV photon energy is due to N $1s \rightarrow \pi^*$ transitions within the peptide-backbone unit.

IV. NEAR-EDGE FINE STRUCTURES

A. N 1*s* absorption edge

The N 1*s* partial x-ray absorption cross section of the pristine protein layer is shown in Fig. 4. No traces of nitrogen were found on the blank substrates indicating that the signal originates from the protein layer exclusively. The NEXAFS is composed of a sharp, though intense π^* resonance at 401.3 eV excitation energy and additional structure in the σ^* region. This spectral shape resembles that given in previous reports on S layers[14,34] and other proteins.[35–39]

The sharp π^* resonance reflects in largest part N $1s \rightarrow \pi^*_{peptide}$ transitions within the peptide group. Experimental and theoretical studies for glycine, diglycine, and triglycine clearly demonstrate the appearance of that intense π^* resonance only after formation of the peptide bond.[35] Moreover, its energy position agrees well with that in previous reports on N 1*s* protein spectra[36–40] where N $1s \rightarrow \pi^*_{peptide}$ transitions largely dominate. On the other hand, when considering isolated amino acids, an N $1s \rightarrow \pi^*$ resonance is observed only for few of them.[41] Amide groups in asparagine (Asn) and glutamine (Gln) give rise to a π^* peak at 400.7 eV. Furthermore, histidine (His), tryptophan (Trp), and arginine (Arg) feature π^* resonances which were attributed to the presence of either planar aromatic structures (His, Trp) or guanidine groups (Arg) in the side chains. However, considering their relative low occurrence in the S-layer molecule, it turns obvious that the vast majority of chemical groups contributing to the observed π^* resonance must be peptide groups (~90%). In good approximation, this resonance can there-

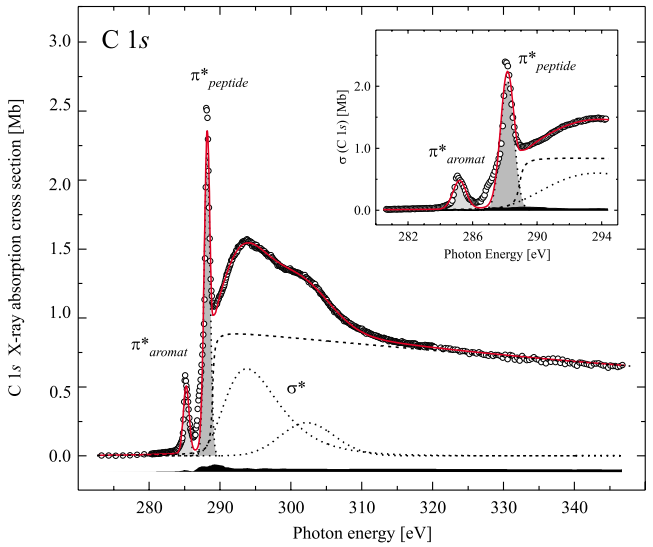

FIG. 5. (Color online) C 1*s* partial x-ray absorption cross section normalized to the contribution of a single carbon atom. The two sharp π^* resonances at 288.1 and 285.0 eV reflect $1s \rightarrow \pi^*$ transitions within the peptide-backbone unit and aromatic protein side chains, respectively. The tiny black-shaded area at the bottom shows the respective C 1*s* absorption by substrate contaminations.

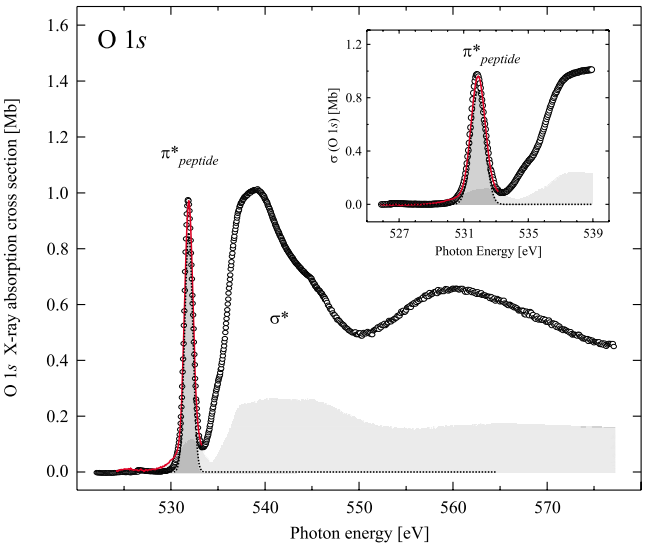

FIG. 6. (Color online) O 1*s* partial x-ray absorption cross section normalized to the contribution of a single oxygen atom. Beside the pristine protein layer the SiO_x substrate makes considerable contribution to the spectrum (~19%, light-gray area). The fit analysis of the $\pi^*_{peptide}$ resonance around 531.8 eV was performed on the difference spectrum of both curves (not shown) which corresponds to x-ray absorption by the pristine protein layer.

fore be identified with N $1s \rightarrow \pi^*_{peptide}$ transitions within the peptide backbone.

In order to estimate its relative intensity we performed a least-squares fit analysis on the N 1*s* NEXAFS spectrum.[42] For the π^* peak a Gaussian-convoluted Lorentzian, i.e., a Voigt line shape, was assumed. Deconvolution of the σ^* region was done using four asymmetric Gaussian line shapes. The continuum step was modeled with an arctan multiplied by an exponential decay function. Obviously, π^* and σ^* resonances do not interfere significantly, which could have possibly tampered fit analysis.

B. C 1*s* absorption edge

The C 1*s* NEXAFS spectrum, normalized to the cross section of one carbon atom, is shown in Fig. 5. Contributions of the SiO_x substrate were estimated from a blank substrate and are included at the bottom as a black area. Obviously, their impact is negligible. Therefore, the measured spectrum can be identified in very good approximation with C 1*s* absorption of the pristine protein layer. The near-edge region features two narrow π^* resonances at 285.0 and 288.1 eV and additional structure in the σ^* range. For the assignment, we refer to the comprehensive experimental and theoretical work published previously.[14,35–38,41,43–45]

The 285.0 eV π^* resonance is observed only for amino acids with aromatic side chains, i.e., Phe, Trp, and Tyr, and hence has been ascribed to aromatic structures (π^*_{aromat}).[41] An intense π^* peak at ~288.5 eV is common to all amino acids and for the most part due to their common structural element, the carboxyl group COO^-. Upon protein formation, the carbonyl groups are incorporated into the peptide-backbone units which comes along with a well-documented redshift of their C $1s \rightarrow \pi^*$ resonance by ~0.4 eV.[4,35,37,38] Accordingly, we observed the sharp intense peak at 288.1 eV excitation energy which is characteristic of C $1s \rightarrow \pi^*_{peptide}$ transitions within the peptide bond. Note, that for isolated amino acids an enhancement of the 288.5 eV peak is observed for Asp, Asn, Glu, and Gln due to additional COO^- or $CONH_2$ groups in the side chains.[41] However, resonances of these groups should not be affected in their energy position upon peptide-bond formation and thus remain at ~288.5–289 eV excitation energy in proteins, too. The same holds for the other side chain π^* resonances showing up at excitation energies between 286 and 287.5 eV.[41] We can, therefore, attribute the 288.1 eV peak to transitions in the peptide backbone exclusively.

In order to extract the intensity of the $1s \rightarrow \pi^*_{peptide}$ peak we deconvoluted the C 1*s* NEXAFS spectrum, similar to how it has been done for the N 1*s* edge. The results are included in the figure. Again, the fit indicates no significant overlap between the π^* and the σ^* regions. At 286–287.5 eV and in a narrow window around 289 eV the fit notably deviates from the data points. This is most likely because, apart from the π^*_{aromat} excitations, the other discussed π^* excitations in the protein side chains were not included into the fit. Therefore absorption in these regions is underestimated.

C. O 1*s* absorption edge

Figure 6 shows the O 1*s* NEXAFS spectrum normalized to the cross section of one oxygen atom. Below the ionization potential it shows a single, rather broad π^* resonance at 531.8 eV, which is typical for all protein spectra.[36–38]

Compared to the N 1*s* and C 1*s* spectra, reliable analysis of the O 1*s* NEXAFS spectrum comes along with considerable uncertainties for several reasons. First, the SiO_x sub-

strate makes a large contribution (~19%) to the detected signal. Second, in the region of O 1*s* excitations nonmonochromatic fractions of the incident photon beam are no longer suppressed because of the limited application range of the Ti filter. Hence the detected electron yield is partly generated by second-order light. Third, even considered in their isolated form, prior to peptide-bond formation, all amino acids show strong O $1s \rightarrow \pi^*$ resonances.[41] However, there is much evidence that, after being assembled into a protein structure, only the amino acids asparagine and glutamine further on contribute to this peak whereas the main share of about 90% is hold by the peptide backbone.[46]

Here, we only account for O 1*s* contributions by the substrate. As stated above, they amount to 19%. The O 1*s* signal measured for a blank SiO_x substrate and rescaled such that it corresponds to 19% continuum intensity of the original signal is included in Fig. 6 as light-shaded area. Beside pronounced intensity in the σ^* region, the spectrum features a broad peak at ~532 eV which strongly interferes with the sharp peptide-bond resonance. The difference spectrum between total signal and substrate signal (not shown) equates x-ray absorption of the pristine protein layer. There we found that the sharp π^* resonance is fully separated from the rest of the spectrum. Hence one can restrict the fit analysis to this small energy window, using only a single peak of Voigt line shape to extract the relative intensity of the $1s \rightarrow \pi^*_{peptide}$ peak.

V. OSCILLATOR STRENGTHS OF THE PEPTIDE BOND

Being the energy integral of the x-ray absorption cross section σ the areas under the $1s \rightarrow \pi^*_{peptide}$ resonance peaks correspond to the oscillator strengths of the respective resonances. Applying Eq. (1) we found that the intensity of the $1s \rightarrow \pi^*_{peptide}$ peaks would equate an oscillator strength of f^*_C=0.0197, f^*_N=0.0108, and f^*_O=0.0083 at the C, N, and O 1*s* edges, respectively. However, it should be noted that these numbers are extracted from spectra which, respectively, reflect an average over all carbon, nitrogen, and oxygen atoms in the S layer. In fact, only part of these atoms participate in the peptide groups, the rest is bound in protein side chains.

If we consider, for instance, the nitrogen species, only 83% of all atoms are part of the peptide units. Accordingly, those peptide-bond nitrogens make a contribution of only 83% in the total spectrum intensity and likewise the N $1s \rightarrow \pi^*_{peptide}$ resonance is downscaled to 83% of the intensity expected for a protein without nitrogen-containing side chains. In order to extract the oscillator strength f_N for a single peptide-backbone unit one must account for this interfering effect of side chain nitrogen. Renormalization to full, 100% intensity yields f_N=0.0130 oscillator strength for N $1s \rightarrow \pi^*_{peptide}$ excitations within the peptide bond of the S-layer protein. Similarly, the C $1s \rightarrow \pi^*_{peptide}$ oscillator strength for a single peptide-backbone unit can be derived by weighting the experimental f^*_C with the relative share of peptide units in all carbon atoms of the protein structure (21%). We thus obtain f_C=0.0938. In order to extract f_O for a single peptide unit we have to account for two points. First, the protein signal makes only 81% of the full absorption intensity, the rest originates from the substrate. Second, 32 at. % of oxygen are bound in protein side chains. Correspondingly only 68% of the protein O 1*s* absorption happens in the peptide-backbone unit. Considering both, we yield f_O =0.0151 for the O $1s \rightarrow \pi^*_{peptide}$ oscillator strength of a single peptide unit.

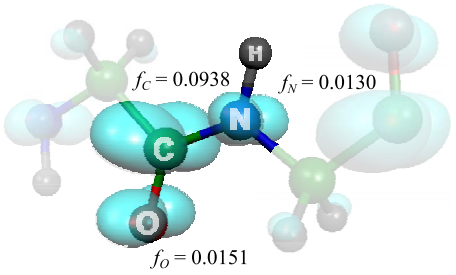

FIG. 7. (Color online) A peptide-backbone unit together with results of a first-principles calculation of the charge distribution related to the $\pi^*_{peptide}$ orbital. The experimentally determined oscillator strengths $f_x(x$=C,N,O) of $1s \rightarrow \pi^*_{peptide}$ excitations clearly correlate with the overlap between the $\pi^*_{peptide}$ orbital and the 1*s* orbital centered on the respective atom.

These oscillator strength values $f_x(x$=C,N,O) are highly informative numbers and closely related to the topology of the $\pi^*_{peptide}$ orbitals. Considering the mathematical expression of *f* derived in dipole approximation and written in position space representation[1]

$$f_{ij} = \frac{2m}{\hbar^2}(E_j - E_i)|\boldsymbol{e}\langle j|\hat{\boldsymbol{r}}|i\rangle|^2 \propto (E_j - E_i)\left|\int d^3\boldsymbol{r}\, r\varphi_j^*(\boldsymbol{r})\varphi_i(\boldsymbol{r})\right|^2 \tag{2}$$

one finds, that the *f* numbers are basically given by the energy separation and the overlap between the initial core-level states $|i\rangle$ and the final $\pi^*_{peptide}$ states $|j\rangle$. The dependence on the polarization $\boldsymbol{e}$ of the electrical field averages out as a constant factor $\propto \int_0^\pi d\vartheta \sin^2\vartheta$ here because of the mentioned statistical orientation of the peptide bonds.[1]

If we identify the energy separation $(E_j - E_i)$ with the photon energy position of the resonance peaks and weight the oscillator strengths, respectively, the remaining differences in the f_x must be related to differing overlap between the $\pi^*_{peptide}$ orbitals and the C, N, and O 1*s* orbitals strongly localized at the carbon, nitrogen, and oxygen sites of the peptide unit. The latter can be approximated with the atomic, spherically symmetric wave functions. Accounting for both the differing energy separations and the decreasing 1*s*-orbital radii when going from the C to the N to the O site of the peptide bond,[47] one can qualitatively estimate from the f_x values that the density of the $\pi^*_{peptide}$ charge should be distributed mostly around the C, less around the O, and least around the N site of the peptide unit.

In Fig. 7 we show results which we obtained from supercell first-principles calculations of the charge distribution related to the $\pi^*_{peptide}$ orbital.[46,48] The calculations were performed for a polyglycine chain in β-sheet conformation. Data calculated for other polyglycine confirmations are simi-

lar to those shown here. Clearly, the $\pi^*_{peptide}$ charge is mainly concentrated around the carbon sites of the peptide-backbone unit whereas the oxygen and especially the nitrogen site show much less overlap, in accordance with what has been estimated from the experimental data.

It should be noted, that generally peptide-bond oscillator strengths will depend on a couple of circumstances and can vary from protein structure to protein structure within certain boundaries. Differences in the oscillator strength of the peptide bond may arise from the fact that the latter must not to be considered as an isolated chemical group. Instead it is influenced, among others, by the chain length of the polypeptide, the residues of neighboring amino acids and the conformation of the protein. For instance, previous experimental and theoretical studies revealed that the oscillator strength of the N $1s \rightarrow \pi^*_{peptide}$ resonance increases with increasing chain length and decreases with growing deviation of the protein backbone from planar geometry.[35]

VI. CONCLUSIONS

Using an elaborated experimental approach we were able to obtain absolute x-ray absorption cross sections for a large protein adsorbed to a solid-state surface. In particular, the oscillator strengths of 1*s* excitations into the peptide-bond orbital with π^* character were determined for all three relevant absorption edges. Comparing with results of first-principles calculations, a close correlation between the intramolecular structure of the protein and its x-ray absorption properties could be evidenced experimentally.

Since all spectra can be obtained in electron-yield mode, no special instrumentation of the experimental end station mounted to the beamline is needed. In fact, our approach can be followed at any dipole beamline after additional measures for light monochromatization are taken. Furthermore, we anticipate that it can be used not only for proteins but for various kinds of surface-adsorbed molecules for which, to our knowledge, determination of absolute cross sections and oscillator strengths has not been considered yet. Note that surface-adsorbed molecules often exhibited a preferred orientation with respect to the surface, resulting in an additional dependence of the resonance intensity on the angle between light polarization and sample.[1] This must be additionally accounted for during data analysis then, however, does not affect the applicability of the here presented approach.

ACKNOWLEDGMENTS

The authors thank A. Preobrajenski (MAX-lab facility, Lund, Sweden) for experimental support and fruitful discussions. This work was financially supported by the DFG (Grants No. ME 1256/13-1, No. MO 1049/5-1, and No. VY 64/1-1) and the bilateral program "Russian-German laboratory at BESSY."

[1] J. Stöhr, *NEXAFS Spectroscopy* (Springer, Berlin, 1992).
[2] D. A. Outka, J. Stöhr, R. J. Madix, H. H. Rotermund, B. Hermsmeier, and J. Solomon, Surf. Sci. **185**, 53 (1987).
[3] W. Wurth, J. Stöhr, P. Feulner, X. Pan, K. R. Bauchspiess, Y. Baba, E. Hudel, G. Rocker, and D. Menzel, Phys. Rev. Lett. **65**, 2426 (1990).
[4] J. Stewart-Ornstein, A. P. Hitchcock, D. Cruz, P. Henklein, J. Overhage, K. Hilpert, J. D. Hale, and R. E. W. Hancock, J. Phys. Chem. B **111**, 7691 (2007).
[5] J. Stöhr, F. Sette, and A. L. Johnson, Phys. Rev. Lett. **53**, 1684 (1984).
[6] J. Stöhr, K. Baberschke, R. Jaeger, R. Treichler, and S. Brennan, Phys. Rev. Lett. **47**, 381 (1981).
[7] R. A. Rosenberg, P. J. Love, and V. Rehn, Phys. Rev. B **33**, 4034 (1986).
[8] J. Stöhr and D. A. Outka, Phys. Rev. B **36**, 7891 (1987).
[9] U. B. Sleytr, P. Messner, D. Pum, and M. Sára, *Crystalline Bacterial Cell Surface Proteins* (Academic, San Diego, 1996).
[10] U. B. Sleytr and M. Sára, Trends Biotechnol. **15**, 20 (1997).
[11] M. Mertig, R. Kirsch, W. Pompe, and H. Engelhardt, Eur. Phys. J. D **9**, 45 (1999).
[12] R. Wahl, M. Mertig, J. Raff, S. Selenska-Pobell, and W. Pompe, Adv. Mater. (Weinheim, Ger.) **13**, 736 (2001).
[13] UNIPROT database (http://www.uniprot.org).
[14] D. V. Vyalikh, A. Kirchner, A. Kade, S. Danzenbächer, Yu. S. Dedkov, M. Mertig, and S. L. Molodtsov, J. Phys.: Condens. Matter **18**, S131 (2006).
[15] S. A. Gorovikov, S. L. Molodtsov, and R. Follath, Nucl. Instrum. Methods Phys. Res. A **411**, 506 (1998).
[16] S. I. Fedoseenko, D. V. Vyalikh, I. F. Iossifov, R. Follath, S. A. Gorovikov, R. Püttner, J. S. Schmidt, S. L. Molodtsov, V. K. Adamchuk, W. Gudat, and G. Kaindl, Nucl. Instrum. Methods Phys. Res. A **505**, 718 (2003).
[17] D. V. Vyalikh, S. Danzenbächer, M. Mertig, A. Kirchner, W. Pompe, Yu. S. Dedkov, and S. L. Molodtsov, Phys. Rev. Lett. **93**, 238103 (2004).
[18] K. Kummer, D. V. Vyalikh, G. Gavrila, A. Kade, M. Weigel-Jech, M. Mertig, and S. L. Molodtsov, J. Electron Spectrosc. Relat. Phenom. **163**, 59 (2008).
[19] M. R. Howells, A. P. Hitchcock, and C. J. Jacobsen, J. Electron Spectrosc. Relat. Phenom. **170**, 1 (2009).
[20] A. Kade, D. V. Vyalikh, S. Danzenbächer, K. Kummer, A. Blüher, M. Mertig, A. Lanzara, A. Scholl, A. Doran, and S. L. Molodtsov, J. Phys. Chem. B **111**, 13491 (2007).
[21] J. J. Yeh, *Atomic Calculation of Photoionization Cross-Sections and Asymmetry Parameters* (Gordon and Breach Science, Langhorne, PE, 1993); J. J. Yeh and I. Lindau, At. Data Nucl. Data Tables **32**, 1 (1985).
[22] V. N. Sivkov, A. S. Vinogradov, S. V. Nekipelov, D. V. Sivkov, D. V. Vyalikh, and S. L. Molodtsov, Opt. Spectrosc. **101**, 724 (2006).
[23] V. N. Sivkov, A. S. Vinogradov, S. V. Nekipelov, D. V. Sivkov, D. V. Vyalikh, and S. L. Molodtsov, Opt. Spectrosc. **102**, 367 (2007).
[24] F. S. Brown, R. Z. Bachrach, and A. Dianconi, Chem. Phys. Lett. **54**, 425 (1978).

[25] D. A. Shirley, Phys. Rev. B **5**, 4709 (1972).
[26] V. N. Sivkov and A. S. Vinogradov, Phys. Solid State **25**, 897 (1983).
[27] S. V. Nekipelov and V. N. Sivkov, Phys. Solid State **36**, 1512 (1994).
[28] W. Gudat and C. Kunz, Phys. Rev. Lett. **29**, 169 (1972).
[29] A. Kotani and S. Shin, Rev. Mod. Phys. **73**, 203 (2001).
[30] R. Nakajima, J. Stöhr, and Y. U. Idzerda, Phys. Rev. B **59**, 6421 (1999).
[31] U. Fano and J. W. Cooper, Rev. Mod. Phys. **40**, 441 (1968).
[32] A. P. Hitchcock and D. C. Mancini, J. Electron Spectrosc. Relat. Phenom. **67**, 1 (1994).
[33] Again, this is valid only for light elements were fluorescent decay of the excited final state does basically not occur.
[34] D. V. Vyalikh, A. Kirchner, S. Danzenbächer, Yu. S. Dedkov, A. Kade, M. Mertig, and S. L. Molodtsov, J. Phys. Chem. B **109**, 18620 (2005).
[35] M. L. Gordon, G. Cooper, C. Morin, T. Araki, C. C. Turci, K. Kaznatcheev, and A. P. Hitchcock, J. Phys. Chem. A **107**, 6144 (2003).
[36] Y. Zubavichus, A. Shaporenko, M. Grunze, and M. Zharnikov, J. Phys. Chem. B **112**, 4478 (2008).
[37] G. Cooper, M. Gordon, D. Tulumello, C. Turci, K. Kaznatcheev, and A. P. Hitchcock, J. Electron Spectrosc. Relat. Phenom. **137-140**, 795 (2004).
[38] Y. Zubavichus, A. Shaporenko, M. Grunze, and M. Zharnikov, J. Phys. Chem. B **111**, 9803 (2007).
[39] B. W. Loo, Jr., I. M. Sauerwald, A. P. Hitchcock, and S. S. J. Rothman, J. Microsc. **204**, 69 (2001).
[40] A. P. Hitchcock, C. Morin, Y. M. Heng, R. M. Cornelius, and J. L. Brash, J. Biomater. Sci. Polym. Ed. **13**, 919 (2002).
[41] Y. Zubavichus, A. Shaporenko, M. Grunze, and M. Zharnikov, J. Phys. Chem. A **109**, 6998 (2005).
[42] D. A. Outka and J. Stöhr, J. Chem. Phys. **88**, 3539 (1988).
[43] K. Kaznacheyev, A. Osanna, C. Jacobsen, O. Plashkevych, O. Vahtras, O. H. Agren, V. Carravetta, and A. P. Hitchcock, J. Phys. Chem. A **106**, 3153 (2002).
[44] J. Boese, A. Osanna, C. Jacobsen, and J. J. Kirz, J. Electron Spectrosc. Relat. Phenom. **85**, 9 (1997).
[45] V. Carravetta, O. Plashkevych, and O. H. Agren, J. Chem. Phys. **109**, 1456 (1998).
[46] D. V. Vyalikh, V. V. Maslyuk, A. Blüher, A. Kade, K. Kummer, Yu. S. Dedkov, T. Bredow, I. Mertig, M. Mertig, and S. L. Molodtsov, Phys. Rev. Lett. **102**, 098101 (2009).
[47] J. T. Waber and D. T. Cromer, J. Chem. Phys. **42**, 4116 (1965).
[48] V. V. Maslyuk, I. Mertig, T. Bredow, M. Mertig, D. V. Vyalikh, and S. L. Molodtsov, Phys. Rev. B **77**, 045419 (2008).